APCVD OF TIN OXIDE COATINGS ON GLASS

Mingheng Li *, John F. Sopko, James W. McCamy

Glass Technology Center, PPG Industries. P.O.Box 11472, Pittsburgh, PA 15238

Abstract

A fundamental framework for APCVD SnO_2 coatings on glass using monobutyltin trichloride as the precursor, developed using CFD in an impinging flow geometry, is presented in this paper. The CFD model explicitly accounts for homogenous reaction in the gas phase, heterogeneous reaction on the glass surface, thermal effect of the impinging jet on the glass, and impinging flow characteristics in the confined coating zone. A comparison of modeling results with experimental data is described. It is shown that the experimentally observed spatial distribution in the deposition rate is successfully captured by the model and the wave shape in the deposition profile can be explained with boundary layer separation. The effect of numerical scheme, reactor-substrate spacing, and glass line speed on the simulated deposition profile is discussed.

Key words: Glass coating, Chemical vapor deposition, Computational fluid dynamics, Tin oxide, Monobutyltin trichloride

1 Introduction

On-line atmospheric pressure chemical vapor deposition (APCVD) is a critical technique used in the glass industry to deposit coatings on float glass and glass containers and is responsible for the industry-wide production of approximately 110 million ft^2/year of value-added products. The primary product produced in this manner utilizes a fluorine-doped SnO_2 layer as a low-emissivity coating. This conductive layer reflects in the far-IR region yielding improved energy performance in architectural applications.

While APCVD is a cost-effective method for on-line coating on glass [10], improvements in process efficiency are expected to result in reduced solid

* Tel: +1-412-820-8520, Fax: +1-412-820-8640, Email: minghengli@ppg.com.

waste generation and disposal, lower raw materials usage, and a reduction in energy consumption. Therefore, significant drivers exist for developing the fundamental understanding of the APCVD process that will lead to an increase in the process efficiency [1]. Generally speaking, the rate and efficiency of APCVD are dependent on reaction kinetics, fluid flow, heat transport and mass transport in the coating zone. An in-depth understanding of such a reaction-transport process requires high-fidelity computational fluid dynamic (CFD) and/or Chemkin models that are able to precisely capture the flow, thermal and kinetic phenomena. Representative examples in this area include simulation of SnO_2 deposition from $SnCl_4$ in a horizontal cold wall APCVD reactor [18], computational modeling of silicon deposition from SiH_4 in a stagnation rotating disk APCVD reactor [11], numerical analysis of TiO_2 deposition from titanium tetra-iso-propoxide (TTIP) in a cold wall impinging APCVD reactor [9], and detailed kinetic modeling of SnO_2 deposition from dimethyltin dichloride [8]. The numerical simulation based on CFD/Chemkin is able to provide quantitative information of flow behavior and species transport, but typically relies to a large extent on the thermodynamic data, reaction mechanism, and transport properties. Monobutyltin trichloride (or MBTC) used for SnO_2 deposition in the glass industry, which is of interest in the current work, has very limited data reported in the literature [3, 4, 12, 16, 17]. While it is experimentally shown that the reaction of MBTC with oxygen is accelerated at the presence of water, the function of water in the decomposition and/or oxidation of MBTC, is not fully understood. To study this deposition process using CFD, it is very important to note that the deposition rate in the on-line APCVD coating on glass should exceed 200 Angstrom/sec in order to meet the thickness requirement of the coated material on the high line speed glass ribbon [14]. This deposition rate is close to the diffusion limit of the precursor, which implies that the deposition process of SnO_2 from MBTC is mainly limited by the flow behavior as well as mass transport in the coating zone and that the effect of reaction kinetics is less important. As a result, the CFD modeling of online APCVD coating on glass can be done with reasonable accuracy without a highly developed reaction mechanism and kinetic data.

The objective of this work is to provide a computational framework for SnO_2 deposition from MBTC. The current model is developed using CFD with an impinging flow geometry, and explicitly accounts for homogenous reaction in the gas phase, heterogeneous reaction on the glass surface, thermal effect of the impinging jet on the glass, and impinging flow characteristics in the confined coating zone. The reaction kinetics are based on a preliminary research conducted by Sandia National Laboratory and PPG Industries, Inc. during the U.S. Department of Energy, Office of Industrial Technologies, Glass Industry of the Future sponsored program [5]; certain kinetic parameters were modified to fit the experimental data. A comparison of CFD model predictions with experimental measurements shows that the experimentally observed spatial distribution in the deposition rate profile is successfully captured by the

model. Especially, the observed wave shape in the deposition profile can be explained with boundary layer separation. Based on this model, parametric analysis is performed to study the effect of numerical scheme, reactor-substrate spacing and glass line speed on the deposition profile.

2 Experimental setup

The experiments of tin oxide deposition from MBTC are conducted in a pilot-scale APCVD reactor with impinging geometry. Figure 1 shows a schematic view of the reactor. The MBTC is delivered from a vaporizer with nitrogen as the carrier gas. The water, which is the accelerant for the reaction of MBTC and oxygen, is vaporized using air as the carrier gas. After being mixed with the diluent nitrogen right before APCVD reactor, the MBTC with nitrogen and water with air are sent to the plenum, and then the V shape zone. After passing the coating zone, where SnO_2 is produced and deposited on the surface of the substrate, the remanent reactants and by-products exit the exhausts to be disposed. Two nitrogen curtains are used on each side of the reactor to avoid the reactants and products escaping from the coating zone to the atmosphere. All the inlet and exhaust gas flow rates and temperatures are regulated by Labview process control software. Each inlet or outlet consists of a plenum and a V shaped zone for boundary layer development with distribution holes in between. The glass substrate is stationary in this pilot reactor. The baseline parameters used in the experiment are given in Table 1.

3 CFD model for SnO_2 deposition

The computational domain consists of the V shape zone, the coating zone and the substrate (see Figures 1 - 3). The plenum is not included because its inclusion will not significantly change the profile of the deposition rate. The differential equations used to describe the flow dynamics and thermal behavior in the coating zone are continuity, momentum balance, energy balance, species transport, ideal gas law etc. While a simplification of constant surface temperature is commonly used in the numerical simulation of CVD process (e.g., [11, 6, 13, 19]), a conjugate heat transfer between the heating plate below the substrate and the fluid above the substrate will more closely match the experimental arrangement. In the current model, this is achieved through coupling of the glass top surface temperature by the convective heat transfer of the impinging jet and the conductive heat transfer within the glass with a fixed temperature at the bottom of the glass. The heat transfer due to radiation is not accounted for in the current model and might be considered

in future work. The temperature and concentration distributions are uniform at all inlets (distribution slots). The zero gradient in concentration normal to the surface are specified for all the surfaces expect the glass top surface. The pressure outlet boundary conditions are specified at the two exhausts (with a fixed temperature of 450 K) and the two side flows (with a fixed temperature of 300 K). The pressure in the exhausts is varied such that the modeled flow rates match the experimental conditions. The wall of the reactor is assumed to maintain a constant temperature of 400 K. The temperature of the reactor surface and the temperature at the exhaust can be optimized based on experimental measurements, however, an adjustment in these temperatures will not have a significant effect on the deposition rate.

The reaction mechanism is based on the collaborative work of Sandia National Laboratory and PPG Industries, Inc. [5], but we have modified the reaction constant for the surface reaction in that work to fit the experimental data. In this reaction mechanism, the MBTC-water complex is formed rapidly as the two species are mixed together, and the MBTC-water complex reacts with oxygen to form SnO_2 on the high temperature glass surface.

gas phase: $C_4H_9SnCl_3(g) + H_2O(g) = C_4H_9SnCl_3(H_2O)(g)$

surface: $C_4H_9SnCl_3(H_2O)(g) + 0.5O_2(g) = SnO_2(s) + 2C_2H_4(g) + 3HCl(g)$

The reaction rates for both gas and surface reactions are expressed as follows

$$R^g = k_0^g \exp(-E_a^g/RT) c_{MBTC}^{\alpha} c_{H_2O}^{\beta} \tag{1}$$

$$R^s = k_0^s \exp(-E_a^s/RT) c_{MBTC-H_2O}^{\alpha} c_{O_2}^{\beta} \tag{2}$$

and the kinetic parameters are listed in Table 2.

The thermodynamical data of MBTC and MBTC-H_2O complex are taken from Sandia National Laboratory [2]. The calculation of heat capacity, viscosity, and thermal conductivity of the mixture is based on the property of pure nitrogen. This is because the nitrogen gas is in excess of 75% and the estimation of these properties of MBTC and MBTC-H_2O complex is avoided. The mass diffusivity of each species is estimated based on kinetic theory, and the Lennard-Jones parameters of each species are given in Table 3.

4 Results and discussions

The process model is implemented into Fluent, a commercial CFD computer program, and is solved by the finite volume method. The governing mass, momentum and energy balance equations together with the ideal gas state equation are solved first using the first-order upwind scheme to obtain a convergent solution and then the second-order upwind scheme to precisely capture the flow characteristics. Generally it requires about 250 iterative steps to reduce the residuals of all the variables to 10^{-5} for the first-order upwind scheme and additonal hundreds of steps for the second-order upwind scheme in each simulation run.

4.1 Modeling results under baseline operating conditions

The simulated contours of velocity, temperature and mole fractions of MBTC, H_2O, MBTC-H_2O complex and HCl in the whole field using the second order upwind scheme under the baseline conditions are shown in Figures 2 and 3. It is shown that with the specified nitrogen curtain flow and exhaust flow, no chemicals escape from the coating zone to the surrounding atmosphere. As the vertical velocity is converted to horizontal velocity, there are two recirculation zones formed in the confined coating zone. One is at the corner of the inlet slot and the other is several slot widths away from the inlet slot. Based on the kinetics of the mechanism used here, the reaction of water with MBTC is so fast that almost all the MBTC is converted to MBTC-H_2O complex immediately as it enters the reactor. On the glass surface, the MBTC-H_2O complex reacts with oxygen to generate SnO_2, which forms the coating layer. The byproduct, HCl, diffuses from the substrate to the gas phase.

The simulated deposition profile of SnO_2 under the baseline operating conditions is shown in Figure 4. The CFD simulation successfully captures the wave shape of the deposition profile, and the deviation of average magnitude of the deposition rate is less than 10% of the corresponding experimental value, indicating that the CFD model with modified kinetic parameters reasonably predicts the deposition rate.

It is consistently found in both experiment and simulation that there is a dip in the center of the deposition rate profile (directly underneath of the inlet slot). There might be several factors that contribute to this phenomenon. Due to the balance of momentum ($P + \frac{1}{2}\rho u^2$), the pressure at the stagnation point is higher than its neighborhood because the flow is stagnant in the center. However, as will be shown later, the thermal interaction between the impinging jet and the glass is the largest in the center and the temperature is the lowest

underneath the inlet slot on the glass surface. According to kinetic theory, the diffusion coefficient ($D \propto T^{1.5}/P$) is the lowest in the center. On the other hand, since the flow is almost zero near the stagnation point, the mass transfer boundary layer is thicker in the center. Recall that $\delta_c \propto x/\sqrt{Re_x} \propto \sqrt{\nu x/u}$, the boundary layer for mass transfer becomes thicker as the velocity decreases. Therefore, the mass transfer coefficient ($h_c \approx D/\delta_c$) is smaller in the center than its neighborhood.

4.2 Influence of numerical scheme on the deposition rate profile

It is shown that the second order upwind scheme gives more accurate results than the first order upwind scheme in the simulation (see Figure 4), even though the residuals of all the iterative variables are reduced to an order of 10^{-6}. While the second order upwind scheme successfully captures the dips in the center and two secondary shapes (dips and humps) between the inlet and exhaust ($x/B \approx$ 5-6, where B is the width of the inlet slot), the first order upwind scheme fails to predicts the secondary shapes. A comparison of the contours of velocity, temperature and mole fraction of MBTC-H_2O in the coating zone with different numerical schemes shows that the first order upwind scheme provides a different description of the flow behavior in the region where the secondary shapes occur (see Figure 6). Nevertheless, the relative difference in the average deposition rate is less than 4% for these two numerical schemes, implying the first order upwind scheme is able to provide a very good estimate of the average deposition rate.

4.3 Influence of reactor-substrate spacing on the deposition rate profile

The deposition profile under reduced reactor-substrate spacing (slot to glass distance) is shown in Figure 7. The CFD simulation successfully captures the deposition rate at each of the measurement points, except for the one in the center. Note that there is also a dip in the deposition profile obtained from the CFD simulation, although it is hard to tell from Figure 7. The average deviation of model prediction at each measurement point from the experimental measurement is only 9.8% and the error of the cumulative deposition rate from modeling accounts for less than 6% of the corresponding experimental value, indicating that the CFD model with modified kinetic parameters reasonably predicts the deposition rate.

The deposition profile is dependent on the reactor-substrate spacing, similar to what is observed in heat transfer in the impinging flow geometry [7]. The difference in the deposition profile occurs in several regions (see Figure 8).

One is directly underneath the inlet slot. This might be caused by a smaller recirculation region in the vicinity of the inlet slot when the reactor-substrate spacing is reduced. Another region is located at several slot widths away from the inlet (see Figure 9), which can be readily explained by boundary layer separation [15]. The boundary layer tends to separate from the surface of the substrate under sufficient increasing fluid pressure downstream of the flow, or known as adverse pressure gradient. When the pressure gradient is large enough such that the shear stress reduces to zero, the separation occurs and the fluid is no longer pulling on the wall, and opposite flow develops to push the boundary layer off of the solid surface. The boundary layer separation is alleviated as the flow area decreases. The third region is close to the exhaust. This is because the velocity parallel to the glass is more uniform in this region and it increases as a result of decreased flow area. Therefore, the boundary layer for mass transfer decreases and the deposition is enhanced.

The surface temperature under different reactor-substrate spacing is shown in Figure 10. In either case, the temperature is the lowest in the center, which indicates that the thermal interaction between the impinging jet and the glass is the largest. Far away from the inlet, conduction from the depth of the glass allows the surface temperature to recover to a higher temperature at the gas glass interface. This phenomenon partially explains the dip in the deposition profile.

4.4 Influence of line speed on the deposition rate profile

All the previous simulations are based on the stagnation geometry. However, in the manufacturing process, the glass is moving with a line speed of around 0.1-0.2 m/sec, which implies that the moving boundary conditions may need to be applied on the glass surface. At high line speed, when moving boundary condition is included, it is found that the velocity field is no longer symmetric. Instead, the flow is more towards downstream of the inlet slot than upstream, as shown in Figure 11. As a result of the asymmetric flow, the deposition rate is higher downstream of the inlet slot than upstream, as shown in Figure 12. The effect of the moving glass on the deposition rate profile is more apparent as the line speed is increased.

4.5 Limitations of current model and future research directions

Regarding the reaction mechanism, we note that when the oxygen is in excess, ethylene might be oxidized to carbon monoxide and carbon dioxide. However, no difference is found in the deposition rate profile after this modification is made. Moreover, while it is observed in experiments that an increase in

water/MBTC ratio will increase the tin oxide deposition, this behavior is not explicitly accounted for in the current mechanism. A hypothesis is that the water vapor might break the the Sn-Cl bond in MBTC (similar to the water-$SnCl_4$ system) to form products with smaller molecular weight. The higher the water/MBTC ratio, the smaller the product molecule and the larger the diffusion flux to the substrate. This mechanism might partially explain the function of water in the tin oxide deposition, and might be tested in the future work.

5 Conclusions

This work provides a computational framework for the APCVD of SnO_2 coatings with MBTC as the precursor. It is shown that the deposition process is mainly diffusion controlled and the effect of reaction kinetics is less important. The wave shape in the deposition profile is due to the several stagnation/recirculation regions in the coating zone.

Acknowledgement

This work is partially supported by the U.S. Department of Energy, Office of Industrial Technologies Glass Industry of the Future team. Discussions with Mark Allendorf at Sandia National Laboratory and Mehran Arbab, Robert Greiner, Guosheng Kang, Thomas Sailock, William Siskos, and Kwang Won at PPG Glass Technology Center are gratefully acknowledged.

Nomenclature

B	Slot width	$[m]$
D	Diffusion coefficient	$[m^2/sec]$
E_a	Activation energy	$[J/mol]$
h_c	mass transfer coefficient	$[mol/m^2 \cdot sec]$
L	Distance from inlet to exhaust	$[m]$
m_0	Total flow rate	$[slm]$
T	Temperature	$[K]$
P	Pressure	$[Pa]$
k_0^g	Reaction constant for the gas phase reaction	$[mol/m^3 \cdot sec]$
k_0^s	Reaction constant for the surface reaction	$[mol/m^2 \cdot sec]$
R	Gas constant	$[8.314 J/mol \cdot K]$
Re	Reynolds number	[-]
x	Axial distance from the center of the inlet slot	$[m]$
u	Velocity	$[m/sec]$
ρ	Density	$[kg/m^3]$
ν	Kinematic viscosity	$[m^2/sec]$

References

[1] M. D. Allendorf. Research needs for coatings on glass. Summary of the U. S. Department of Energy roadmapping workshop. *Thin Solid Films*, 392:155–163, 2001.

[2] M. D. Allendorf. Personal communication, 2004.

[3] J. L. Buchanan and C. McKown. Off-line sheet glass coating system. *Journal of Non-Crystalline Solids*, 218:179–184, 1997.

[4] Y. Chae, W. G. Houf, A. H. McDaniel, J. Troup, and M. D. Allendorf. Stagnation flow reactor investigation of tin oxide CVD from monobutyltin trichloride. *Journal of the Electrochemical Society*, 151:C527–C534, 2004.

[5] D. Dauson and M. D. Allendorf. Development of process optimization strategies, models, and chemical databases for on-line coating of float glass. In *Glass Industry of the Future Team Program Review Meeting*, Washington, D. C., June 2004. http://www.eere.energy.gov/industry/glass/pdfs/p_1640.pdf.

[6] A. Ern, V. Giovangigli, and M. D. Smooke. Detailed modeling of three-dimensional chemical vapor deposition. *Journal of Crystal Growth*, 180:670–679, 1997.

[7] R. Gardon and J. C. Akfirat. Heat transfer characteristics of impinging two-dimensional air jets. *Journal of Heat Transfer, ASME Transactions*, 88:101–108, 1966.

[8] C. J. Giunta, D. A. Strickler, and R. G. Gordon. Kinetic modeling of the chemical vapor deposition of tin oxide from dimethyltin dichloride and oxygen. *Journal of Physical Chemistry*, 97:2275–2283, 1993.

[9] S. A. Gokoglu, G. D. Stewart, J. Collins, and D. E. Rosner. Numerical analysis of an impinging jet reactor for the CVD and gas-phase nucleation of titania. In S. B. Desu, D. B. Beach, B. W. Wessels, and S. Gokoglu, editors, *Material Research Society Symposium Proceedings*, volume 335, pages 171–176, 1994.

[10] R. Gordon. Chemical vapor deposition of coatings on glass. *Journal of Non-Crystalline Solids*, 218:81–91, 1997.

[11] C. R. Kleijn. Computational modeling of transport phenomena and detailed chemistry in chemical vapor deposition - a benchmark solution. *Thin Solid Films*, 365:294–306, 2000.

[12] S. M. Lee, D. L. Kim, H. J. Youn, and K. S. Hong. Tin oxide films by chemical vapor deposition using a monobutyltin trichloride source: The effect of H_2O on deposition behavior and electrical properties. *Japanese Journal of Applied Physics*, 39:407–412, 2000.

[13] G. Luo, S. P. Vanka, and N. Glumac. Fluid flow and transport processes in a large area atmospheric pressure stagnation flow CVD reactor for deposition of thin films. *International Journal of Heat and Mass Transfer*, 47:4979–4994, 2004.

[14] R. J. McCurdy. Successful implementation methods of atmospheric CVD on a glass manufacturing line. *Thin Solid Films*, 351:66–72, 1999.

[15] H. Schlichting and K. Gersten. *Boundary Layer Theory*. Springer, Berlin, Germany, 8th edition, 2000.

[16] A. M. B. van Mol. *Chemical Vapour Deposition of Tin Oxide Thin Films*. PhD thesis, TNO, The Netherlands, 2003.

[17] A. M. B. van Mol, Y. Chae, A. H. McDaniel, and M. D. Allendorf. Chemical vapor deposition of tin oxide: Fundamentals and applications. *Thin Solid Films,* in press, 2005.

[18] T. C. Xenidou, A. G. Boudouvis, D. M. Tsamakis, and N. C. Markatosa. An experimentally assisted computational analysis of tin oxide deposition in a cold-wall APCVD reactor. *Journal of the Electrochemical Society*, 151:C757–C764, 2004.

[19] Z. Yuan, S. Mokhtari, A. Ferdinand, J. Eakin, and L. Bartholomew. Optimization of SiO_2 film conformality in TEOS/O_3 APCVD. *Thin Solid Films*, 290-291:422–426, 1996.

Table 1
Reference operating conditions for tin oxide deposition.

N_2 carrier flow rate (slm)	20
N_2 dilute flow rate (slm)	45
N_2 curtain flow rate (slm)	45 (each)
Air flow rate (slm)	20
Exhaust flow rate (slm)	95 (each)
MBTC concentration (mol%)	0.4
H_2O concentration (mol%)	3
Inlet gas temperature (K)	436
Substrate temperature at the bottom (K)	922
Coater height (inch)	0.25

Table 2
Kinetic parameters in the gas and surface reaction [5].

Reaction	α	β	k_0 (mol/m^3/sec)	E_a (J/mol/K)
gas	1	1	4×10^{14}	10^4
surface	1	1	2.5×10^{2} *	1.37×10^4

* modified from 10^{10}.

Table 3
Lennard-Jones parameters of the chemical species.

Chemical species	σ (Å)	ϵ/k (K)	Reference
C_2H_4	3.971	280.8	
$C_4H_9SnCl_3$	5.5	528.069	[2]
$C_4H_{11}SnCl_3O$	4.5525	549.78	[2]
H_2O	2.605	572.4	
N_2	3.621	97.53	
O_2	3.458	107.4	
SnO_2	4.534	586.983	

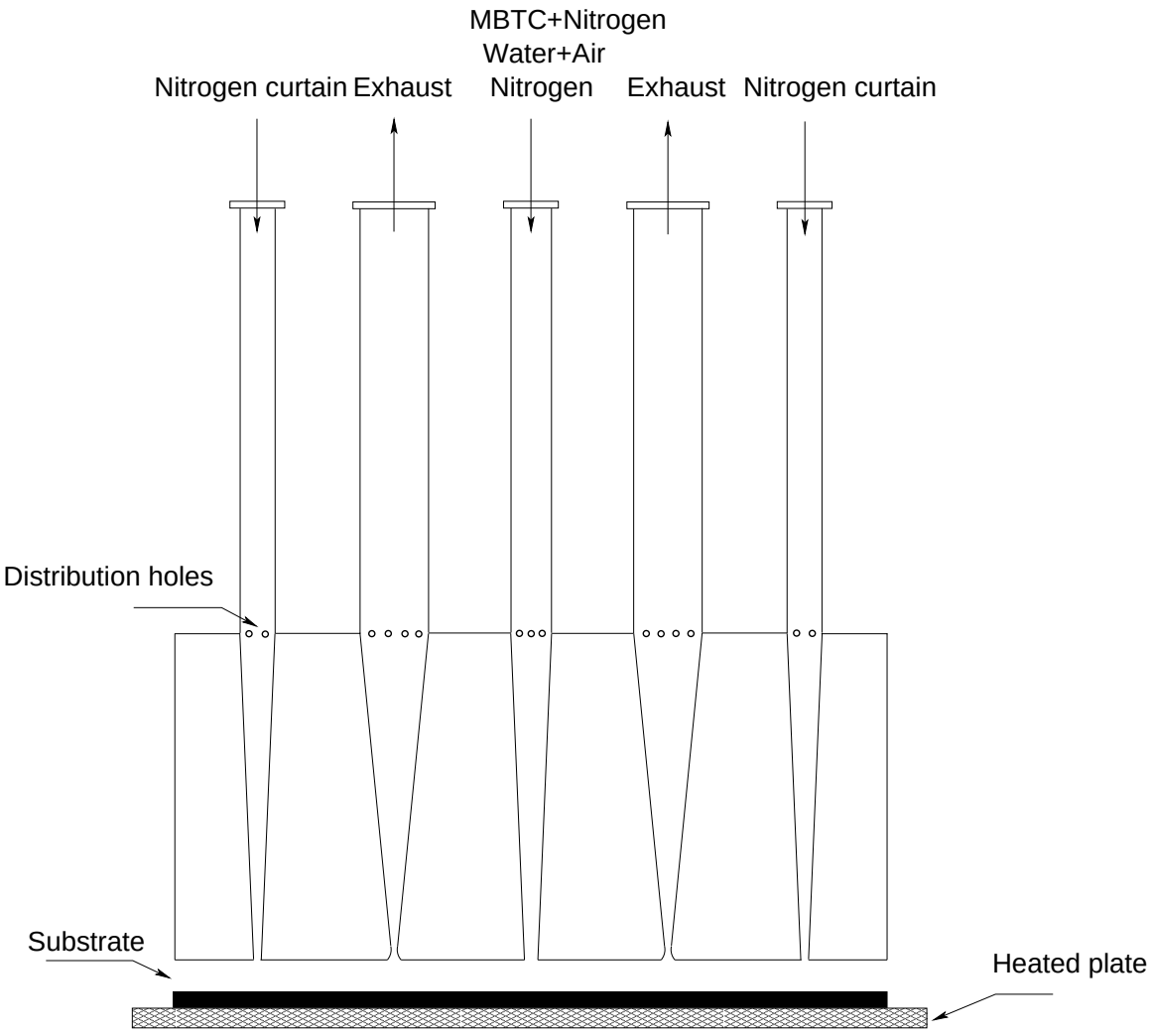

Fig. 1. Schematic of the pilot-scale APCVD reactor (not to scale).

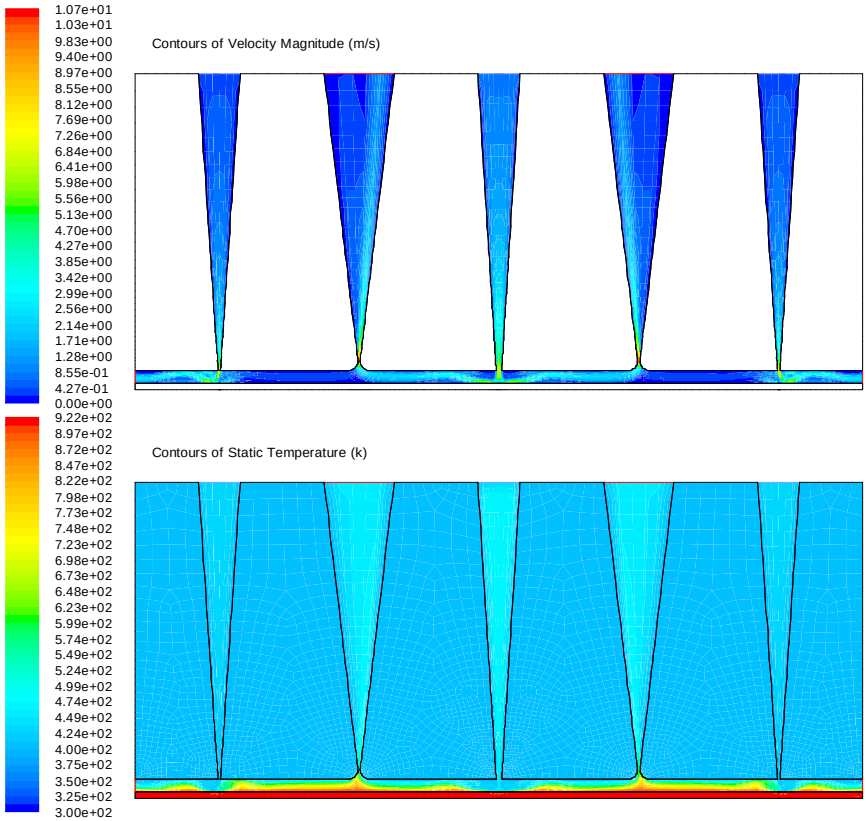

Fig. 2. Contour of velocity magnitude and temperature under reference operating conditions, solved using second order upwind scheme.

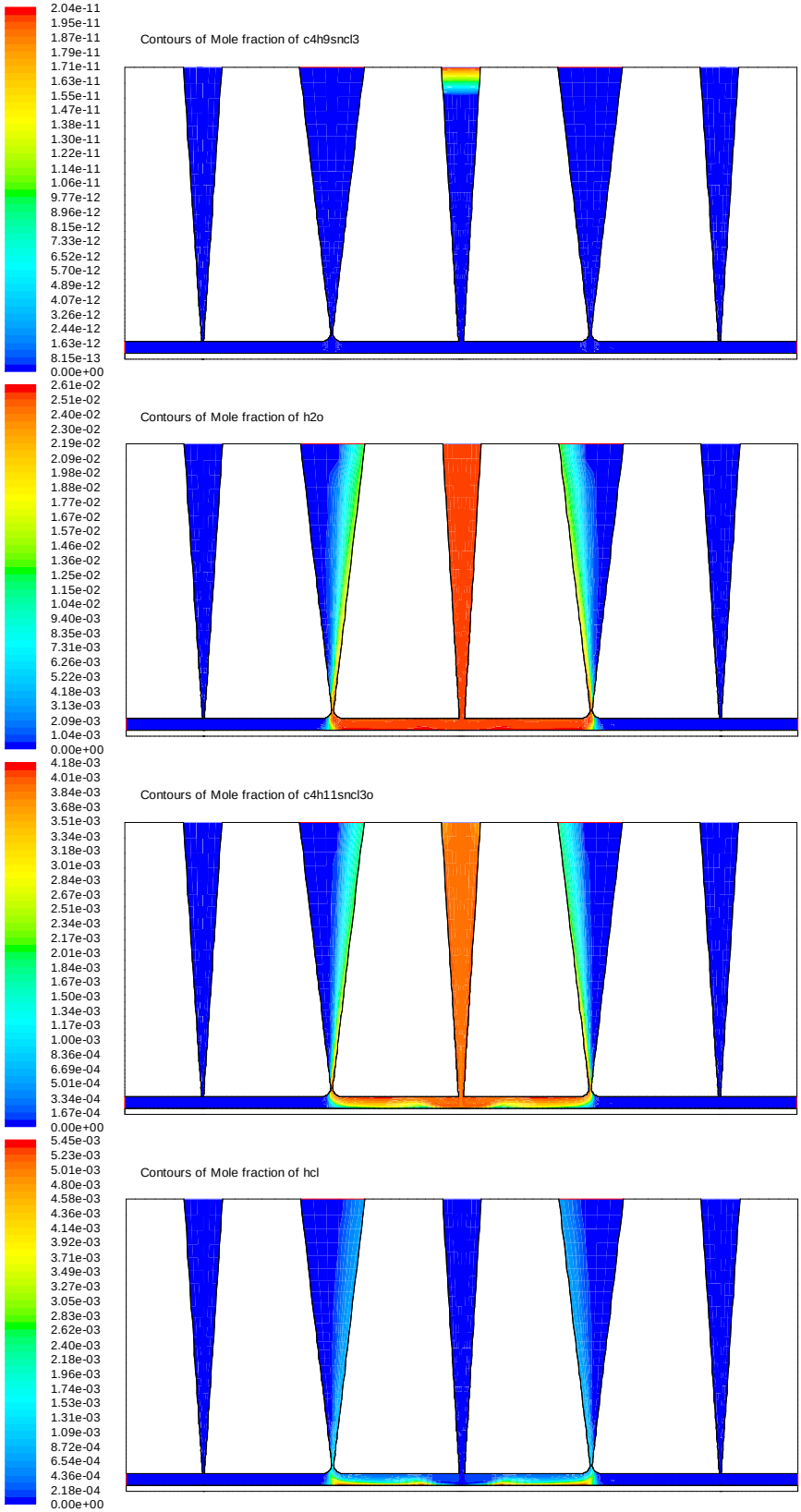

Fig. 3. Contour of MBTC, H_2O, MBTC-H_2O complex and HCl under reference operating conditions, solved using second order upwind scheme.

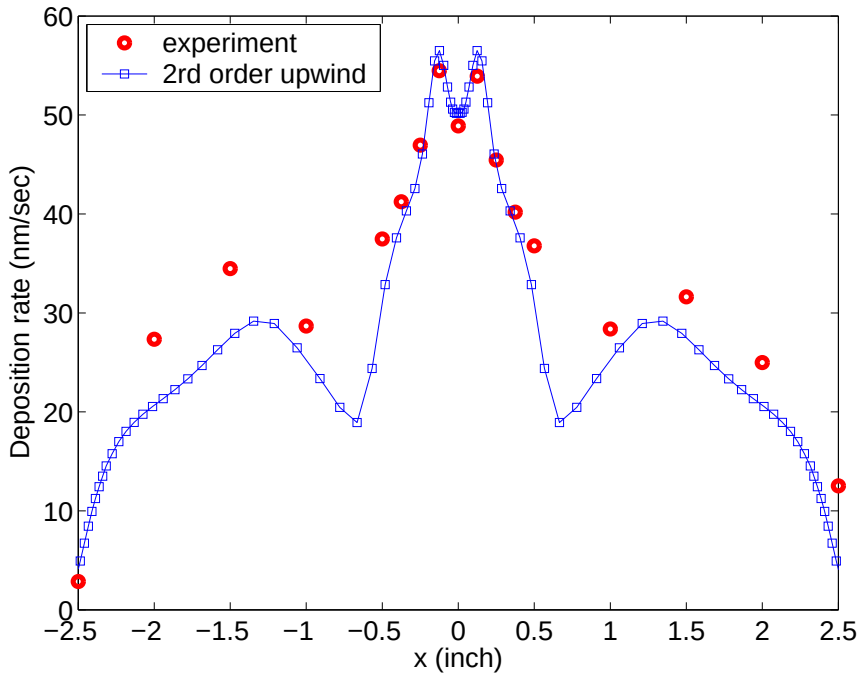

Fig. 4. Comparison of deposition rate profile simulated using the second order upwind scheme scheme with experimental data measured at the reference operating conditions.

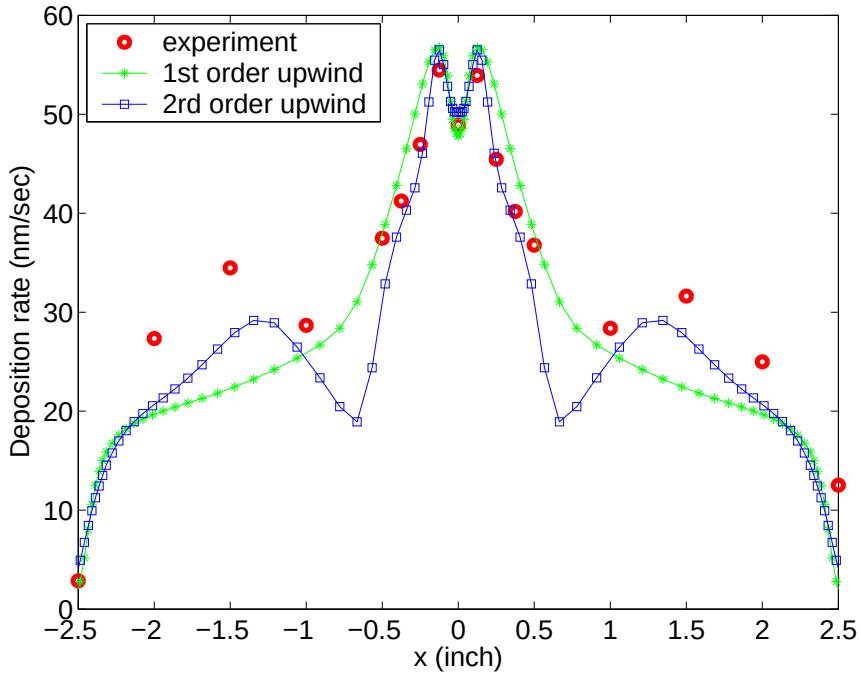

Fig. 5. Comparison of deposition rate profile simulated using different numerical schemes.

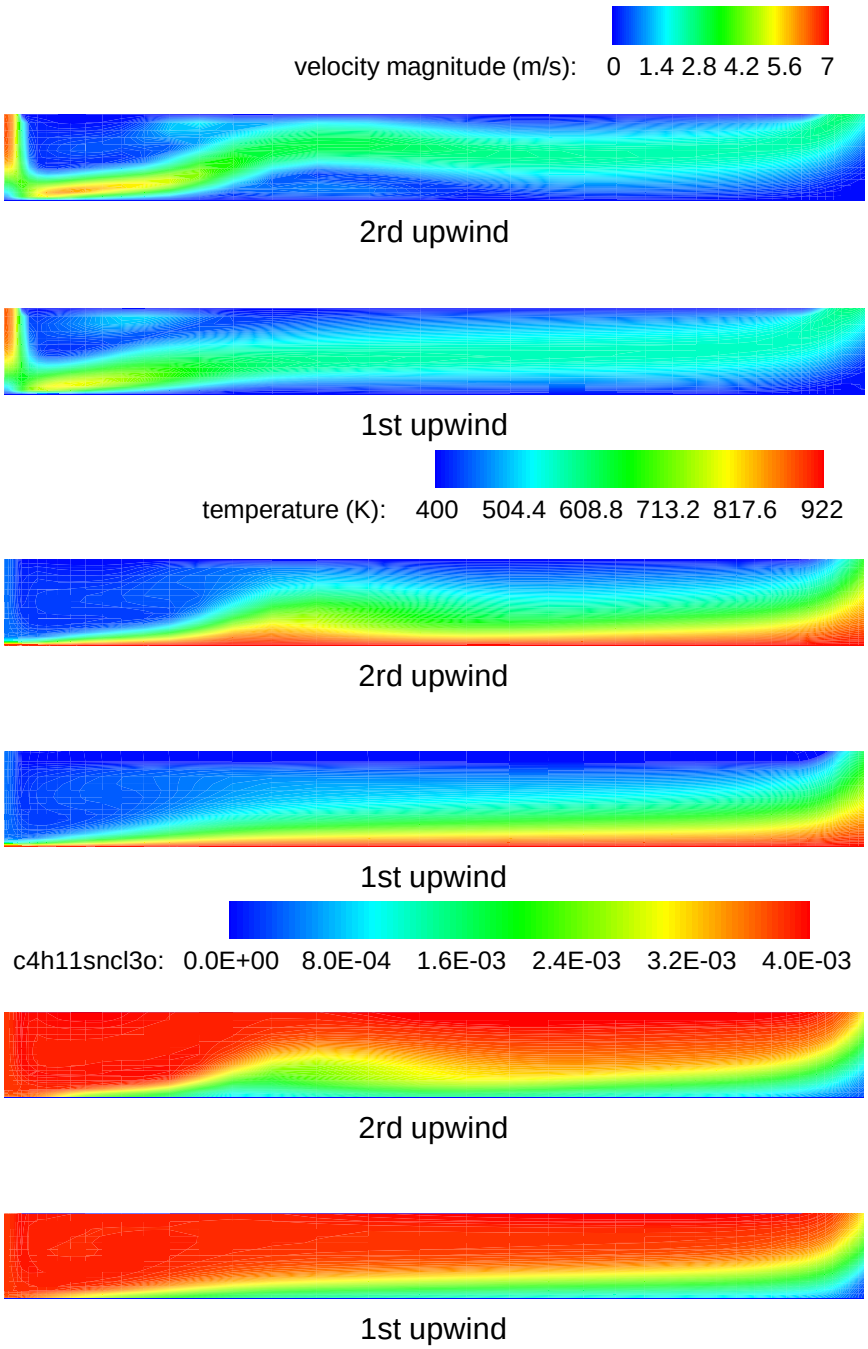

Fig. 6. Contours of velocity magnitude, static temperature and MBTC-H_2O mole fraction solved using different schemes.

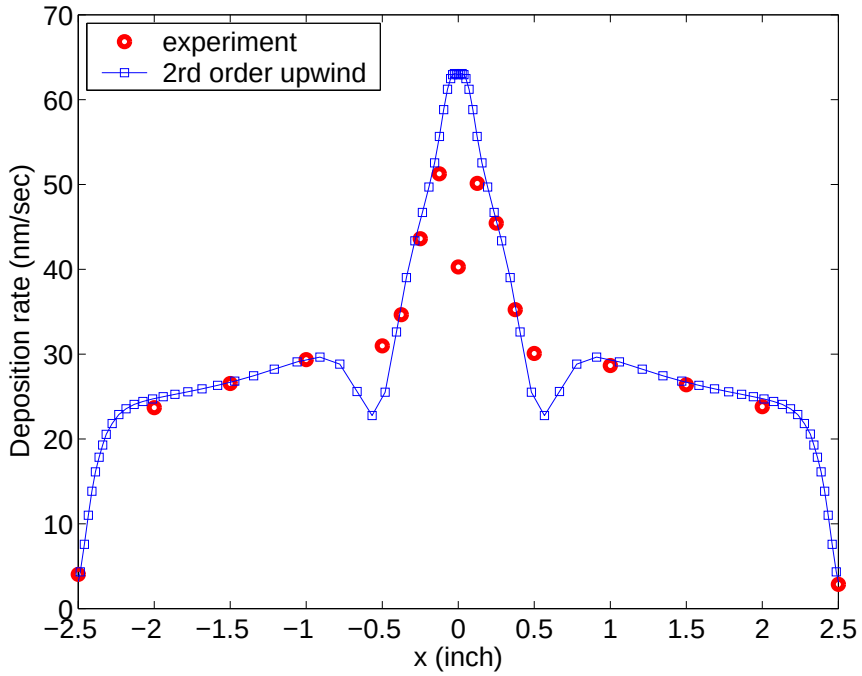

Fig. 7. Comparison of deposition rate profile simulated using the second order upwind scheme scheme with experimental data measured at reduced reactor-substrate spacing (H = 0.15 inch).

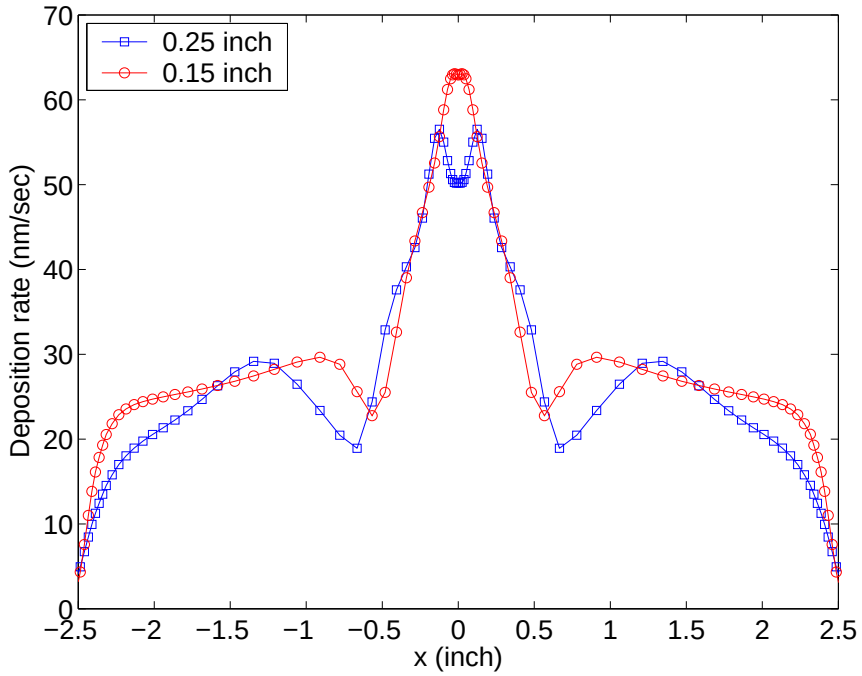

Fig. 8. Influence of reactor-substrate spacing on the deposition rate profile.

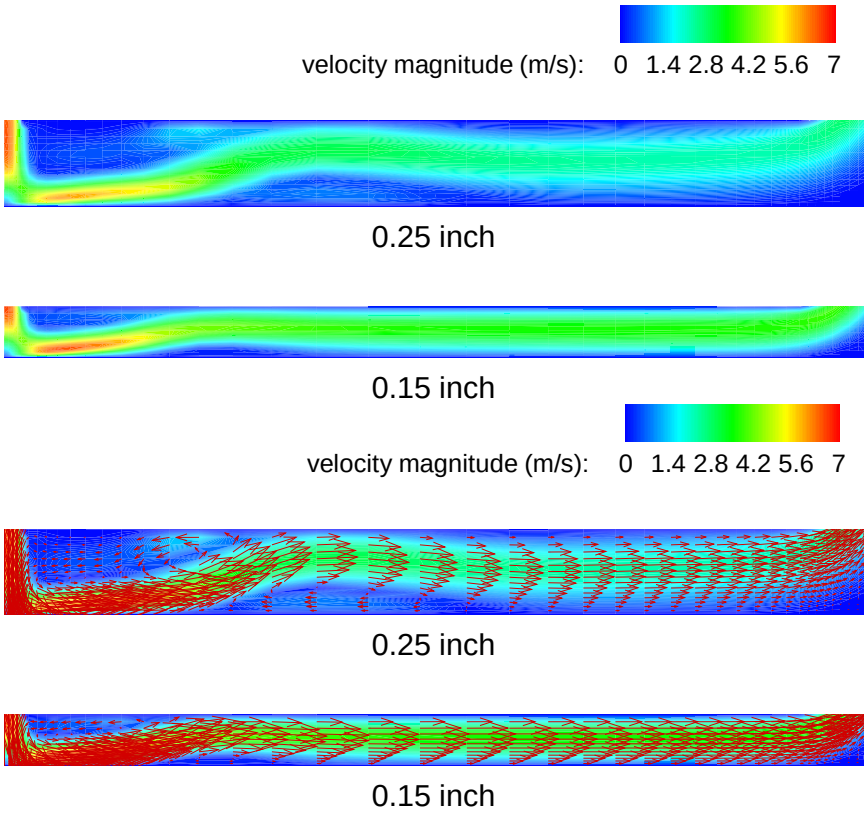

Fig. 9. Influence of reactor-substrate spacing on the velocity flow field.

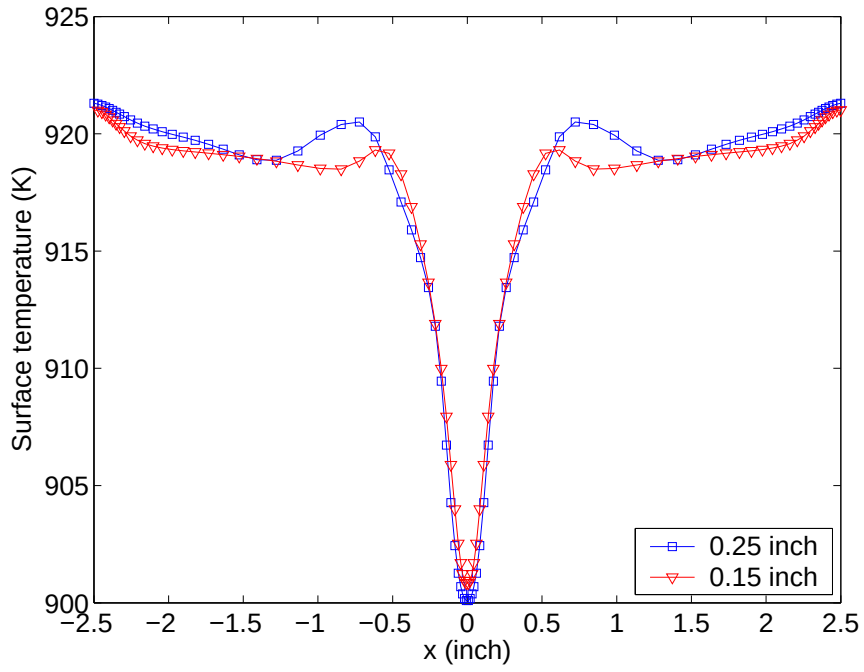

Fig. 10. Influence of reactor-substrate spacing on the substrate surface temperature.

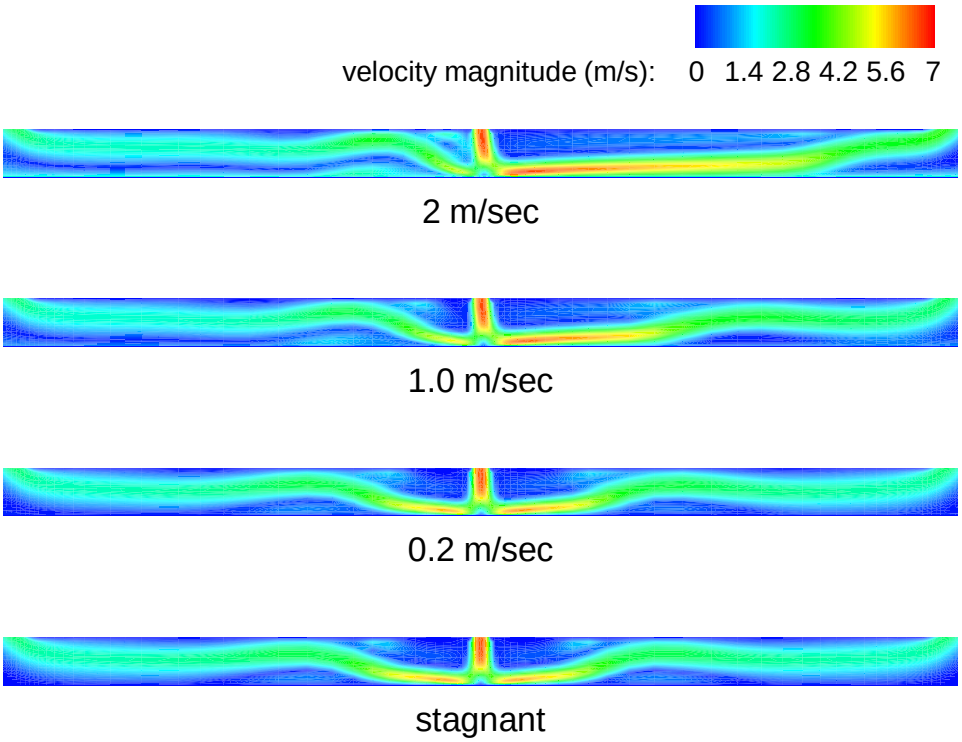

Fig. 11. Influence of glass line speed on the velocity flow field.

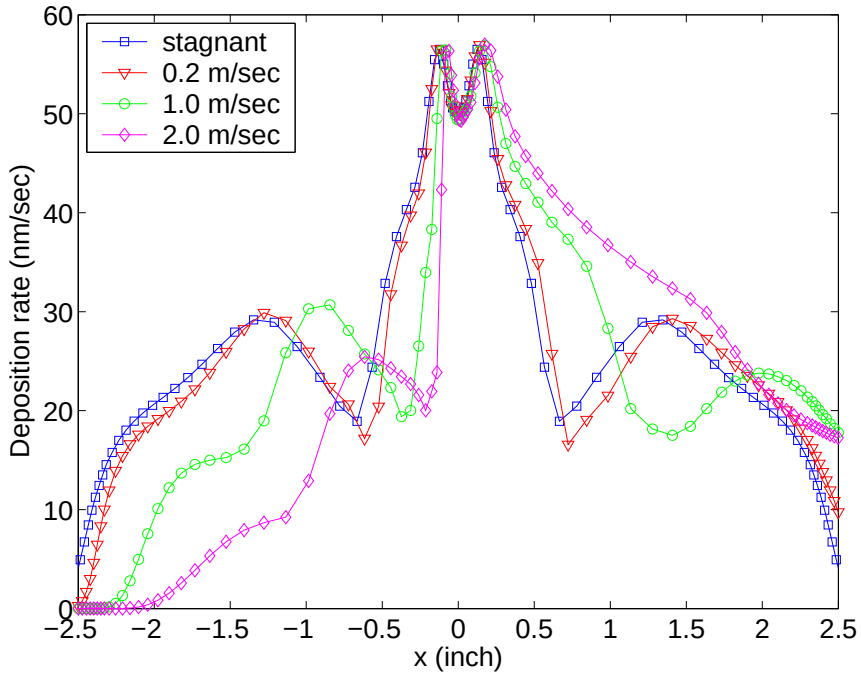

Fig. 12. Influence of glass moving speed on the deposition rate profile.